

# Extracting the Fine Structure of the Left Cardiac Ventricle in 4D CT Data

## A Semi-Automatic Segmentation Pipeline

Juliane Dinse<sup>1</sup>, Daniela Wellein<sup>1</sup>, Matthias Pfeifle<sup>2</sup>, Silvia Born<sup>1</sup>, Thilo Noack<sup>3</sup>,  
Matthias Gutberlet<sup>3</sup>, Lukas Lehmkuhl<sup>3</sup>, Oliver Burgert<sup>1</sup>, Bernhard Preim<sup>4</sup>

<sup>1</sup>VCM/ICCAS, Universität Leipzig

<sup>2</sup>Neurochirurgische Klinik, Universitätsklinikum Tübingen

<sup>3</sup>Herzzentrum Leipzig

<sup>4</sup>Institut für Simulation und Graphik, Otto-von-Guerike-Universität Magdeburg

[daniela.wellein@medizin.uni-leipzig.de](mailto:daniela.wellein@medizin.uni-leipzig.de)

**Abstract.** We propose a pipeline for the segmentation of the left cardiac ventricle (LV) in 4D CT data based on the random walker (RW) algorithm. A segmentation of the LV allows to extract clinical relevant parameters such as ejection fraction (EF) and volume over time (VoT), supporting diagnostic and therapy planning. The presented pipeline works aside approaches incorporating annotated databases, statistical shape modeling or atlas-based segmentation. We have tested our segmentation approach on six clinical 4D CT datasets including different pathologies and typical artifacts and compared the segmentation results to manually segmented slices. We achieve a minimum sensitivity of 86% and specificity of 96%. The resulting EF and VoT is comparable to known reference values and reflects the present pathologies correctly. Additionally, we tested three different routines for thresholding the RW probability maps. An interview with surgical and radiological experts together with high sensitivity scores indicates the superiority of the fixed threshold selection method – especially in the presence of pathologies. The segmentation is also correct near problematic fine structures such as cardiac valves, papillary muscles and the apex of the heart.

## 1 Introduction

A segmentation of the left cardiac ventricle (LV) in 4D CT data is necessary for a functional analysis of the heart. Clinical parameters are often approximated and/or only estimated in end-diastole and end-systole. With the opportunity to measure the ejection fraction (EF) and the volume over time (VoT), diagnostics and therapy planning can be supported. For such an analysis the correct segmentation of cardiac fine structures such as the valves, the papillary muscle (PM), the apex and the heart's inner myocardium, is important.

For the segmentation of the LV various approaches exist. Jolly et al. combine edge, region and shape information for the segmentation of the left ventricle in MRI [1]. Zheng et al. use a database of models and an automatic fitting

to segment all four cardiac chambers in CT data [2]. For the fitting they use manually defined landmarks to deform the control points of the models according to the data. Kirisli et al. propose a multi-atlas-based segmentation of the whole heart in 3D CTA data [3]. They match atlas information and data using a non-rigid registration framework.

Unlike the presented segmentation approaches, we focus on a correct segmentation of the above mentioned cardiac structures. The proposed semi-automatic pipeline allows the inspection (and correction) of all intermediate results to incorporate expert knowledge of the segmenting radiological and surgical experts.

## 2 Materials and Methods

We evaluated our segmentation pipeline on six clinical 4D CT datasets with 10 or 20 time steps. The dimensions of the datasets have been  $512 \times 512 \times 254 \pm 111$  and pixel size was  $0.36\text{-}0.58\text{mm}$  with a slice distance of  $0.67\text{-}1.00\text{mm}$ . The pathologies present in the datasets include coronary artery disease, aortic stenosis, and restricted, dilated, and hypertrophic cardiomyopathy (cardiac muscle is too less/too much compacted). Two of the datasets included a metallic mitral valve replacement, and therefore a high degree of metal artifacts.

The proposed pipeline has been integrated into the volume data processing and visualization platform *VolV* [4] which has already been applied to segmentation in neurosurgical intervention planning [5]. The pipeline consists of three main steps: pre-processing, random walker (RW), and post-processing (Fig. 1). Pre-processing includes anisotropic filtering [6] and an edge enhancement filtering, implemented as the difference image between the original and the mean filtered data. The main step of the pipeline is the RW algorithm, which is formulated on a graph and has strong connections to electrical circuit and potential theory. Its input are labeled voxels belonging to two classes: LV and non-LV structure, i.e. background. The algorithm analytically determines the probability that a random walker starting at each unlabeled voxel will first reach one of the pre-labeled voxels [7]. Output of RW is a probability map in which each voxel is assigned to the label with the highest probability. To initialize the pipeline (Fig. 1), the user has to label a few voxels of the LV and all other anatomical structures (background) only for  $t = 1$ . The labeling does not require any delineation of object boundaries and can be inexact, and, therefore quick.

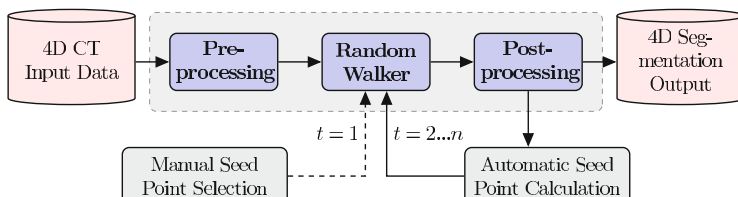


**Fig. 1.** The segmentation pipeline for extracting the LV in 4D CT data.

In the post-processing step, the RW probability map is thresholded to generate the final LV segmentation for the current time step. We used three different thresholding approaches: a manual threshold selection, fixing the threshold to a specific probability and calculating the minimum in the histogram of each time step. Also, a set of labeled seed points for the next time step is generated by reducing the segmentation results of the LV and the background with multiple erosions.

For evaluation, three slices in every time step of each of the six datasets (capturing the valves, the papillary muscles, and the cardiac apex) have been manually segmented, which leads to an overall number of  $3 * 90 = 270$  slices. The sensitivity (SE) and specificity (SP) for each dataset and each thresholding method is computed. The volume over time and the ejection fraction together with its mean squared error to the manual segmentation ( $MSE_{EF}$ ) are calculated and compared to known reference values. In an interview, four surgical/radiological experts have ranked the segmentation results of the different thresholding methods and rated them according to the correct detection of the previously mentioned fine structures.

### 3 Results

Figure 2 shows the segmentation results for three exemplary datasets in the coronal view. The SE and SP for the three different thresholding routines are depicted in Figure 3. The manual thresholding results in an average SE of 91.8% ( $\pm 6.9$ ) and SP of 97.7% ( $\pm 1.2$ ). Fixed thresholding achieves a SE of 94.1% ( $\pm 3.8$ ) and SP of 96.7% ( $\pm 2.2$ ). The minimum thresholding approach leads to an average SE of 88.6% ( $\pm 9.1$ ) and SP of 98.4% ( $\pm 1.2$ ). In Figure 4 the VoT for three exemplary datasets is shown. EF for all datasets is depicted in Table 1.  $MSE_{EF}$  of our method is 2.2% ( $\pm 1.4$ ) for manual thresholding, 2.2% ( $\pm 2.5$ ) for fixed thresholding, and 4.3% ( $\pm 3.6$ ) for minimum thresholding.

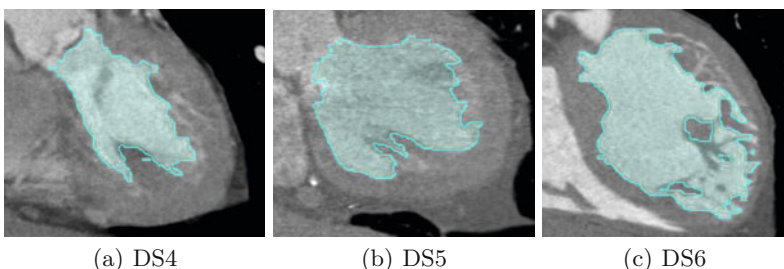


**Fig. 2.** Segmentation of three exemplary datasets showing different pathologies: (a) restricted, (b) hypertrophic, and (c) dilated cardiomyopathy. The interior of the LV as well as fine structures like the aortic outflow tract and papillary muscles are correctly detected.

In the interview the clinical experts preferred the segmentation results of the fixed threshold routine in four out of six datasets. They also confirmed the overall correct detection of the cardiac fine structures.

## 4 Discussion

The previously given SE and SP values correlate with the expert ratings, which indicate, that in our case three manually segmented slices might be enough to measure the segmentation quality. A high SE and SP with a low standard deviation lets us conclude, that the performance is constantly high throughout all tested datasets. The VoT curves (Fig. 4) reflect the general pump (dys-)function of the present pathologies. In DS4 the restrictive cardiomyopathy leads to a delay in proper blood filling in the diastole. This results in a decreased slope of the VoT for the second half of the heart cycle.

The obtained EF values also reflect the underlying pathologies. In DS6 the EF is below 50% for the fixed thresholding. A value, that corresponds to the present dilated cardiomyopathy, in which the amount of blood being pumped out of the LV in the diastole is reduced. In addition, we compared the  $MSE_{EF}$  to the results presented by Zheng et al. [2]. On six datasets with 10 time steps each, they obtained an  $MSE_{EF}$  of 2.3% ( $\pm 1.6$ ). Our  $MSE_{EF}$  of 2.2% for fixed thresholding is comparable, but one has to mention, that this measure is computed in relation to only three manually segmented slices, which might not be enough to deduce the volume of the LV.

In some of the datasets, the plane of the mitral valves, that delineates the LV, is not correctly detected with our pipeline. The dysfunction of the mitral valve leads to the leaflets hitting the cardiac wall and, therefore, they are not detected in the segmentation. In addition, the rapid and inconsistent movement of the

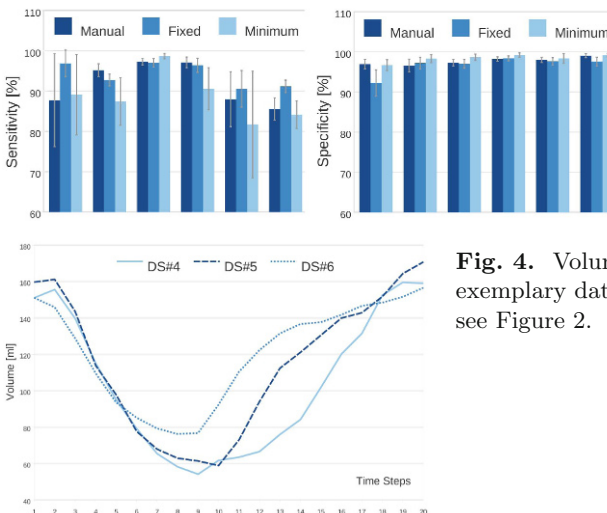


**Fig. 3.** Sensitivity and specificity for the applied thresholding routines and all datasets.

**Fig. 4.** Volume over time curves for three exemplary datasets. For present pathologies see Figure 2.

**Table 1.** The calculated ejection fraction of all datasets (in %).

| Segmentation    | DS1  | DS2  | DS3  | DS4  | DS5  | DS6  |
|-----------------|------|------|------|------|------|------|
| Manual          | 47.6 | 61.5 | 51.9 | 63.4 | 58.2 | 47.5 |
| Manual Thresh.  | 48.8 | 62.1 | 52.8 | 60.9 | 62.2 | 51.1 |
| Fixed Thresh.   | 54.5 | 62.9 | 52.2 | 60.6 | 59.1 | 46.6 |
| Minimum Thresh. | 50.5 | 61.5 | 58.3 | 66.3 | 68.6 | 50.8 |

mitral valve makes them undetectable in some datasets and, the segmentation leaks into the atrium. Furthermore, the PM could be wrongly segmented as belonging to the LV, when the connections between myocardium and PM are too small in the datasets or the contrast between those two structures is too high (PM not dark enough).

To conclude, our pipeline provides a segmentation of the LV that is independent from atlas or large database information. The segmentation quality is high also in the presence of pathologies and artifacts and is able to correctly detect cardiac fine structures. These findings could also be confirmed in an interview with clinical experts.

A promising future work approach would be to use the grey value frequencies in a weighting function for the RW. This was proposed by Grady and Jolly [8], who have shown that their approach outperforms purely intensity-based weighting functions.

## References

1. Jolly MP. Combining edge, region, and shape information to segment the left ventricle in cardiac MR images. *Lect Notes Computer Sci.* 2010; p. 482–90.
2. Zheng Y, Barbu A, Georgescu B, et al. Four-chamber heart modeling and automatic segmentation for 3-D cardiac CT volumes using marginal space learning and steerable features. *IEEE Trans Med Imaging.* 2008;27(11):1668–81.
3. Kirisli HA, Schaap M, Klein Sea. Fully automatic cardiac segmentation from 3D CTA data: a multi-atlas based approach. *Proc SPIE.* 2010;7623:762305–1.
4. Pfeifl M, Born S, Fischer J, et al. VolV - Eine OpenSource-Plattform für die Medizinische Visualisierung. *Proc CURAC.* 2007; p. 193–6.
5. Wellein D, Pfeifl M, Althuizes M, et al. A cortex segmentation pipeline. *Proc BVM.* 2010; p. 271–5.
6. Perona P, Malik J. Scale-space and edge detection using anisotropic diffusion. *IEEE Trans Pattern Anal Mach Intell.* 1990;12(7):629–39.
7. Grady L. Random walks for image segmentation. *IEEE Trans Pattern Anal Mach Intell.* 2006;28(11):1768–83.
8. Grady L, Jolly MP. Weights and topology: a study of the effects of graph construction on 3D image segmentation. *Med Image Comput Comput Assist Interv.* 2008; p. 153–61.